DR YAQIONG WANG (Orcid ID : 0000-0001-8000-608X)

Article type : Rapid Communication

Relaxor behaviour and photocatalytic properties of $BaBi_2Nb_2O_9$

Wenzhi Qi[1], Yaqiong Wang[2*], Jiyue Wu[2], Zimeng Hu[2], Chenglong Jia[1], Giuseppe Viola[2],
Hongtao Zhang[3], Haixue Yan[2]

[1] *Key Laboratory for Magnetism and Magnetic Materials of MOE, Lanzhou University, Lanzhou 730000, P. R. China*

[2] *School of Engineering and Materials Science, Queen Mary University of London, Mile End Road, London E1 4NS, United Kingdom*

[3] *Department of Materials, Loughborough University, Leicestershire, LE11 3TU, United Kingdom*

*Corresponding author

Y. Wang's email: yaqiong.wang@qmul.ac.uk

Abstract

Lead-free Aurivillius phase $BaBi_2Nb_2O_9$ powders were prepared by solid-state reaction. Ferroelectric measurements on $BaBi_2Nb_2O_9$ ceramics at room temperature provided supporting evidence for the existence of polar nanoregions and their reversible response to an external electric field, indicating relaxor behaviour. The photocatalytic degradation of rhodamine B reached 12 % after 3 h irradiation of $BaBi_2Nb_2O_9$ powders under simulated solar light. Ag nanoparticles were photochemically deposited onto the surface of the $BaBi_2Nb_2O_9$ powders and found to act as electron traps, facilitating the separation of photoexcited charge carriers; thus, the photocatalytic performance was significantly improved. The present study is the first examination of the photochemical reactivity of a relaxor ferroelectric within the Aurivillius family with polar nanoregions.

Keywords: $BaBi_2Nb_2O_9$, Aurivillius phase, Relaxor ferroelectric, Polar nanoregions, Photocatalytic properties.

1. Introduction

The urgent demand for solving the problems of rapid consumption of limited fossil fuel reserves and worsening global environment has stimulated an upsurge in research on the development of photocatalysts. Photocatalysts can efficiently convert solar energy into hydrogen energy by splitting water molecules and decompose organic pollutants from industrial effluent through chemical redox reactions driven by photoexcited charge carriers in an excited semiconductor.[1, 2] However, traditional semiconductor photocatalysts, such as TiO_2, CdS and WO_3, suffer from fast charge recombination, which greatly limits their wide application.[3, 4, 5] Therefore, it is urgent to explore novel photocatalysts to solve the energy crisis and environmental pollution issues. Ferroelectric oxides with a perovskite structure, such as $BaTiO_3$ and $BiFeO_3$, have emerged as promising candidates for photocatalysts.[6, 7] Their built-in internal electric fields can enhance the transport of photoinduced charge carriers and thus accelerate their separation.[8, 9] Consequently, their photocatalytic activities can be improved. Moreover, when noble metals (such as Ag, Au, Pt, *etc*.) are deposited onto the surface of photocatalysts as a co-catalyst, their photocatalytic activity can be further enhanced.[6, 10] Noble metal nanoparticles can enhance light absorption due to a surface plasmon resonance (SPR) and extend the charge carrier lifetime by working as 'electron traps' and separating photoexcited electrons and holes; this separation leads to improved photocatalytic efficiency of co-catalyst/semiconductor photocatalysts.[10]

Relaxor ferroelectrics (RFEs) are a special category of ferroelectric. Compared to normal ferroelectrics, they exhibit a broad, frequency-dependent anomaly at the temperature (T_m) of the dielectric peak and a small remnant polarisation.[11, 12] RFEs have been proposed for various applications, such as energy storage capacitors, piezoelectric actuators, ultrasonic transducers, *etc*.[13, 14] However, there are very few studies of their photocatalytic properties. Taïbi *et al.* converted $BaTiO_3$ into an RFE by using various dopants, such as Bi, Y, Sc, Nb, *etc*.[15, 16] Compared to undoped $BaTiO_3$, the modified compositions exhibited larger dielectric constants and wider space charge regions, which resulted in an improved photocatalytic activity.[15, 16] In addition to perovskite structures, photocatalytic activity was also reported for RFEs with a tetragonal tungsten bronze structure, such as strontium barium niobate ($Sr_{0.6}Ba_{0.4}Nb_2O_6$).[17] It is technically important to explore novel RFE-based photocatalysts with various crystal structures to gain a better understanding for the design of materials with enhanced photocatalytic activity.

Aurivillius phase oxides have been attracting increasing interest as lead-free ferroelectric materials due to their superior polarisation fatigue resistance and high Curie points, which make them suitable for non-volatile memory and high-temperature piezoelectric applications.[18, 19, 20] Recent studies have demonstrated photocatalytic activity for Aurivillius ferroelectric oxides such as Bi_2WO_6,[21] Bi_3TiNbO_9,[22] $SrBi_2Ta_2O_9$,[23] $Bi_4Ti_3O_{12}$,[24] $Bi_{5-x}La_xTi_3FeO_{15}$ ($x = 1, 2$).[25] However, to the best of our knowledge, there is no report for the photocatalytic properties of Aurivillius phase RFEs and the effect of noble metal deposition on their photocatalytic behaviour.

$BaBi_2Nb_2O_9$ (BBNO) is a typical Aurivillius phase oxide with RFE behaviour.[26, 27] Previous studies of the crystal structure of BBNO based on synchrotron powder X-ray diffraction[28] and neutron diffraction[29] show that although the macroscopic symmetry of BBNO is tetragonal with the *I4/mmm* space group, a partial mixing of Ba and Bi cations occurs on their respective sites, causing local cation disorder. Structure refinement results indicate that 13.4–20 % of the Ba^{2+} cations are located in the $(Bi_2O_2)^{2+}$ layers.[28,29] Such an inhomogeneous distribution of cations and local charge imbalance suggests weak interaction between polarisation clusters across the perovskite-like layers and the formation of polar nanoregions (PNRs).[30] Kholkin *et al*. [30] obtained polarisation-electric field (*P-E*) loops for BBNO ceramics at three different temperatures (-180 °C, 0 °C, and 100 °C) with a maximum electric field amplitude (E_{max}) of 20 kV/cm and frequency of 1 Hz. They did not find any evidence for ferroelectric domain switching in the hysteresis loops. In this paper, the crystal structure and ferroelectric properties of BBNO were re-investigated. The existence of PNRs in BBNO ceramics was experimentally confirmed. Subsequently, the photocatalytic behaviour of BBNO in the photodegradation of an organic dye, Rhodamine B (RhB), was investigated under simulated solar light. We can expect to achieve improved photocatalytic performance of BBNO by the deposition of Ag nanoparticles. Therefore, Ag nanoparticles were deposited onto the surface of BBNO powders (thereafter referred to as “BBNO-Ag”) and the photocatalytic activity of BBNO-Ag was evaluated.

2. Experimental

Conventional solid-state reaction was used to prepare BBNO. The starting materials included Nb_2O_5 (99.9 %), Bi_2O_3 (99.975 %), and $BaCO_3$ (99 %). A stoichiometric mixture of the oxides was thoroughly milled and calcined at 950 °C for 4 h. To reduce the size of the agglomerates formed during calcination, the calcined BBNO powders were re-milled for 24 h. The as-milled BBNO powders were used for photocatalytic property measurements and for fabricating ceramics for electrical characterization. The pressed pellets were sintered at 1100 °C for 1 h. The density of the sintered BBNO ceramics was 96.9 %. Ag nanoparticles were deposited onto the surface of the as-milled BBNO powder by following a photoreduction method reported elsewhere.[6, 31] In particular, 0.5 g of BBNO powder was placed into a Petri dish with 50 ml of 0.01 M $AgNO_3$ solution. The mixture was then stirred to make a homogeneous deposition, followed by irradiation under a UV illumination source (UV Cube with a high-pressure Hg lamp, Honle) for 10 s. The as-obtained products were separated from the solution by centrifuging with a speed of 4000 rpm for 15 min. The BBNO-Ag powders were collected after being washed by DI water and dried at room temperature.

The crystal structure of the as-milled BBNO powders was identified using X-ray diffraction (XRD, Panalytical Xpert Pro diffractometer) with Cu-K_α radiation. The morphology of the as-milled BBNO powders was observed using a scanning electron microscope (SEM, FEI Inspect F). The composition and chemical states of BBNO-Ag were studied by X-ray photoelectron spectroscopy (XPS, Thermo Scientific™ Nexsa™) with an Al K_α X-ray source. The signal due to C1s from adventitious carbon with a binding energy of 284.8 eV was used to calibrate all the binding energies. Laser diffraction (Zetasizer Nano, Malvern Instruments Ltd, UK) was used to measure the particle size distribution of the as-milled BBNO powders. The ferroelectric *P-E* (polarisation - electric field) and *I-E* (current - electric field) loops were measured at 25 °C and 200 °C with triangular electric field waveforms of various amplitudes and a frequency of 10 Hz using a ferroelectric hysteresis measurement tester (NPL, UK). The optical absorption spectra for BBNO and BBNO-Ag powders were obtained using a UV-Vis spectrophotometer (PerkinElmer LAMBDA 950). The photocatalytic activity of BBNO and BBNO-Ag powders was investigated via the degradation of a Rhodamine B (RhB, 99.99 %) dye solution. In particular, 0.15 g of catalyst powder was mixed with 50 ml of 10 ppm dye solution in a glass Petri dish. The mixture was kept in the dark under constant stirring for 30 min before being placed under a solar simulator (Newport, class ABB). The irradiation intensity was kept at 1 sun (100 mW/cm^2), which was calibrated using a silicon reference solar cell (Newport, Model: 91150V). Photocatalytic decolourisation of RhB using UV blocking and visible light blocking filters was also conducted. Samples with a volume of 2 ml were collected from the solutions at a fixed interval of 30 min and centrifuged at 10,000 rpm for 15 min to remove the photocatalyst powders.

3. Results and discussion

A typical XRD pattern of the as-milled BBNO powders is shown in Fig. 1. The powders showed a single phase within the sensitivity of the XRD equipment. All diffraction peaks can be well indexed by the non-polar tetragonal structure with the *I4/mmm* space group (JCPDS no 40-355).[32] As shown in Fig. 2, the particle size distribution of the as-milled BBNO powders is characterized by three peaks at approximately 0.25, 0.95 and 5.5 µm, with 0.95 µm being the dominant particle size. The inset of Fig. 2 shows a typical SEM image of the as-milled BBNO powders, which indicates an irregular morphology with a broad particle size distribution, ranging from 0.2 µm to 5.6 µm.

The temperature dependence of the dielectric constant and loss for BBNO ceramics at different frequencies reported in our previous study evidenced typical relaxor ferroelectric behaviour.[27] By using dielectric constant data at 1 MHz, the Burns temperature (T_B) was determined to be 628 K (355 °C). T_B is the temperature below which PNRs start to form within the paraelectric matrix due to an inhomogeneous distribution of cations and local charge imbalance.[28, 29, 30] In addition, the frequency dependence of T_m in BBNO ceramics obeys the Vogel-Fulcher law.[33] The value of the freezing temperature T_f obtained from the fitting was 100 K (-173 °C).[27] The details for the determination of the T_B and T_f values are provided in the supplementary information. In the temperature range between T_f and T_B, dipolar fluctuations occur within PNRs. Meanwhile, below T_f, there is not enough thermal energy so that all dipolar motion freezes out.[32]

Fig. 3 illustrates *P-E* and *I-E* loops for BBNO ceramics measured at 10 Hz at two different temperatures (200 °C and 25 °C). The hysteresis loops obtained at 200 °C close to T_m (241 °C at 1 MHz)[27] indicate lossy dielectric behaviour [Fig. 3(a)]. No current peaks associated with ferroelectric domain switching or field-induced rotation and/or growth for PNRs were detected, even though E_{max} was as high as 89 kV/cm. In contrast, in the *I-E* loops generated at 25 °C with E_{max} ranging from 20 to 80 kV/cm, as shown in Fig. 3(b), discernible current humps (or broad peaks) can be observed. To more clearly visualize the details for these current humps, the *I-E* loops in both the first and second quadrants in Fig. 3(b) were replotted, as shown in Fig. 3(c). Fig. 3(c) unambiguously demonstrates that with increasing E_{max}, the current humps broaden and shift along the two green dotted arrows. We believe that the current humps observed in the *I-E* loops in Fig. 3(b) and 3(c) provide experimental support for the existence of PNRs in BBNO ceramics. It is well known that RFEs do not exhibit cooperative long-range ferroelectric order.[33] As previously discussed, in BBNO ceramics, PNRs are formed within the non-polar paraelectric phase with a tetragonal *I4/mmm* structure below T_B (355 °C). PNRs are highly mobile between T_f (- 173 °C) and T_B (355 °C) due to the thermal energy. When the BBNO ceramics were tested at 200 °C, which is close to T_m, the strong thermal motion of PNRs disrupted the alignment of their polarisation along the electric field direction. Thus, no current peaks are present in the *I-E* loops [Fig. 3(a)]. As the temperature is decreased to 25 °C, reversible electric field-induced rotations and growth of PNRs may occur under an applied electric field. PNRs can be oriented along the electric field direction and enlarged during electrical loading, giving rise to the current peaks in the 1st and 3rd quadrants of the *I-E* loops. However, this metastable electric field-induced polar state returns to its initial state during unloading, determining the presence of the current peaks in the 2nd and 4th quadrants of the *I-E* loops. Analogous observations of current humps in *I-E* loops were previously reported for other RFEs including both Aurivillius[34] and perovskite structures.[35, 36, 37, 38] Kholkin *et al*. did not find any field-induced switching event in the *P-E* loops of BBNO ceramics generated at three different temperatures (-180 °C, 0 °C, and 100 °C) with an electric field amplitude of E_{max} = 20 kV/cm,[30] which is probably due to the much lower E_{max} (≤ 20 kV/cm) compared to that used in our work (80 - 89 kV/cm). As a result, this is the first time that supporting evidence is reported for the existence of PNRs within BBNO ceramics and their dynamic response to an external electric field.

Both SEM (Fig. S2) and XPS (Fig. S3) results indicate successful deposition of Ag nanoparticles onto the surface of the BBNO powders. UV-Vis absorption spectra for the BBNO and BBNO-Ag powders are shown in Fig. 4(a). The BBNO powders show a main absorption in the UV light range. The incorporation of Ag nanoparticles increased the light absorption of the photocatalysts in the visible region due to SPR.[10] Fig. 4(b) shows the derived Tauc plot for the BBNO powders. The optical band gap (E_g) of the BBNO powders can be calculated by the Tauc equation:[39]

$$(ahv)^{\mathrm{n}} = A(hv - E_g) \qquad (1)$$

where a is the measured absorption coefficient, h is the Planck's constant, v is the frequency of light, A is a proportional constant, and E_g is the bandgap. n is 0.5 and 2 for indirect band gap and direct band gap materials, respectively. E_g can be obtained from the tangent line in a plot of $(ahv)^2$ against photon energy. Based on a fitting using equation (1), the band gap of BBNO is estimated to be direct with a value of 3.2 eV.

The photodegradation of RhB under different irradiation conditions was used to evaluate the photocatalytic properties of both BBNO and BBNO-Ag powders, as shown in Fig. 4(c). The data show that 12 % of RhB degraded after BBNO powders were irradiated by full light for 3 h. However, BBNO-Ag powders showed a significantly enhanced photocatalytic activity, with nearly 100 % RhB degradation achieved within the same duration. The good photocatalytic activity of BBNO-Ag powders can be attributed to the following reasons: (1) Ag nanoparticles can act as electron traps to enhance the separation of electrons and holes, and, therefore, increase the photocatalytic activity of BBNO-Ag;[6, 10] (2) The enhanced visible light absorption of BBNO-Ag due to the SPR effect from Ag nanoparticles possibly enables improvement of the photocatalytic reaction rates by transferring the absorbed energy to BBNO.

To study the effect of increased visible light absorption on the photocatalytic activity of BBNO-Ag powders, photocatalytic decolourisation of RhB using UV blocking and visible light blocking filters was conducted. When BBNO-Ag powders were placed under UV blocking irradiation, no degradation of RhB was observed. Meanwhile, a complete RhB degradation was achieved under visible light blocking irradiation within the same duration, showing tiny differences in the profile under full light irradiation. The present results clearly indicate that the enhanced RhB degradation rate obtained by the incorporation of Ag nanoparticles on the BBNO powder surface is not caused by photoexcited charge carriers generated from visible light absorption due to SPR. Instead, the enhanced RhB degradation rate can be mainly attributed to the increased charge separation at the photocatalyst surface. A schematic diagram of the proposed charge transfer process in BBNO-Ag is shown in Fig. S4.[40]

The Fermi energy level of noble metals (like Ag) is usually lower than the lowest energy level of the conduction band of semiconductors (like BBNO in this paper). The photoexcited electrons in the conduction band of BBNO will move to the Ag nanoparticles, which act as electron traps and catalytic sites for reduction reactions.[10, 40]

4. Conclusions

In summary, for the first time, our study relates the photocatalytic activity in a relaxor ferroelectric within the Aurivillius family to the presence of PNRs. BBNO powders with an average size of 0.95 μm were prepared via conventional solid-state reaction. The as-milled BBNO powders showed a non-polar tetragonal structure with the *I4/mmm* space group. The freezing temperature T_f and the Burns temperature T_B for BBNO were identified at -173 °C and 355 °C, respectively. The observation of slim *P-E* loops and discernible current humps/peaks in the *I-E* loops for the BBNO ceramics at 25 °C support the existence of PNRs and their dynamic response under an electric field. UV-Vis light spectroscopy suggested that the direct band gap of BBNO is 3.2 eV. The photocatalytic degradation of rhodamine B reached 12 % after BBNO powders were irradiated under solar simulated light for 3 h. The deposition of Ag nanoparticles onto the surface of BBNO is beneficial to the separation of photoexcited charge carriers at the photocatalyst surface. Therefore, a significantly enhanced photocatalytic degradation of up to 100 % was achieved after BBNO-Ag powders were irradiated under the same conditions and for the same duration. All results indicate that combining a relaxor ferroelectric BBNO with plasmonic metal nanoparticles, such as Ag, is a promising strategy to fabricate high-performance photocatalysts.

Acknowledgement

Dr. Yaqiong Wang would like to acknowledge the Chinese Scholarship Council for supporting this work.

References

1. Chen C, Ma W, Zhao J. Semiconductor-mediated photodegradation of pollutants under visible-light irradiation. Chem Soc Rev. 2010; 39: 4206-4219.

2.. Gholipour MR, Dinh C.-T, Béland F, Do T.-O. Nanocomposite heterojunctions as sunlight-driven photocatalysts for hydrogen production from water splitting. Nanoscale. 2015; 7: 8187-8208.

3. Daghrir R, Drogui P, Robert D. Modified TiO_2 for environmental photocatalytic applications: a review. Ind Eng Chem Res. 2013; 52: 3581-3599.

4. Fresno F, Portela R, Suárez S, Coronado JM. Photocatalytic materials: recent achievements and near future trends. J Mater Chem A. 2014; 2: 2863-2884.

5. Tachibana Y, Vayssieres L, Durrant JR. Artificial photosynthesis for solar water-splitting. Nat Photonics. 2012; 6: 511.

6. Cui Y, Briscoe J, Dunn S. Effect of Ferroelectricity on Solar-Light-Driven Photocatalytic Activity of $BaTiO_3$ - Influence on the Carrier Separation and Stern Layer Formation. Chem

Mater. 2013; 25: 4215-4223.

7. Cao D, Wang Z, Nasori, Wen L, Mi Y, Lei Y. Switchable Charge-Transfer in the Photoelectrochemical Energy-Conversion Process of Ferroelectric $BiFeO_3$ Photoelectrodes. Angew Chem. 2014; 126: 11207-11211.

8. Li L, Salvador PA, Rohrer GS. Photocatalysts with internal electric fields. Nanoscale. 2014; 6: 24-42.

9. Morris MR, Pendlebury SR, Hong J, Dunn S, Durrant JR. Effect of Internal Electric Fields on Charge Carrier Dynamics in a Ferroelectric Material for Solar Energy Conversion. Adv Mater. 2016; 28: 7123-7128.

10. Linic S, Christopher P, Ingram DB. Plasmonic-metal nanostructures for efficient conversion of solar to chemical energy. Nat Mater. 2011; 10: 911.

11. Al-Aaraji MN, Hall DA. Influence of $K_{0.5}Bi_{0.5}TiO_3$ on the structure, dielectric and ferroelectric properties of (Ba, Ca)(Zr, Ti)O_3 ceramics. J Eur Ceram Soc. 2018; 38: 2344-2352.

12. Bormanis K, Satarov S, Kalvane A, Sternberg A, Burkhanov AI. Shil'nikov AV. Diffuse phase transitions in lead containing relaxor ferroelectrics: Bias field effects. Ferroelectrics. 2003; 296: 169-174.

13. Levy M, Vanga R, Moon KS, Park HK, Hong YK. Single-crystal relaxor ferroelectric piezoactuators with interdigitated electrodes. IEEE T Ultrason Ferr. 2004; 51: 1593-1599.

14. Lee HJ, Zhang S, Luo J, Li F, Shrout TR. Thickness‐Dependent Properties of Relaxor‐$PbTiO_3$ Ferroelectrics for Ultrasonic Transducers. Adv Funct Mater. 2010; 20: 3154-3162.

15. Haddadou N, Bensemma N, Rekhila G, Trari M, Taïbi K. Photoelectrochemical properties of the relaxor $Ba(Ti_{0.90}Sc_{0.05}Nb_{0.05})O_3$: application to the degradation of amoxicillin under solar light. J Mater Sci-Mater in Electronics. 2018; 29: 5042-5048.

16. Kerfah A, Taïbi K, Omeiri S, Trari M. Relaxor ferroelectric and photocatalytic behaviour of $Ba_{0.785}Bi_{0.127}Y_{0.017}TiO_3$ composition. Sol Energy. 2011; 85: 443-449.

17. Barnes E, Alberts EM, Mimun LC, Brame JA, Warner CM, Harmon AR, Poda AR. Photoinduced Metallic Particle Growth on Single-Crystal Relaxor Ferroelectric Strontium Barium Niobate. J Phys Chem C. 2018; 122: 5590-5598.

18. Yan H, Zhang H, Ubic R, Reece MJ, Liu J, Shen ZJ. Orientation dependence of dielectric and relaxor behaviour in Aurivillius phase $BaBi_2Nb_2O_9$ ceramics prepared by spark plasma sintering. J Mater Sci-Mater in Electronics. 2006; 17: 657-661.

19. Hong SH, Trolier-McKinstry S, Messing GL. Dielectric and electromechanical properties

of textured niobium‐doped bismuth titanate ceramics. J Am Ceram Soc. 2000; 83: 113-118.

20. Park B, Kang B, Bu SD, Noh TW, Lee J, Jo W. Lanthanum-substituted bismuth titanate for use in non-volatile memories. Nature. 1999; 401: 682.

21. Kudo A, Hijii S. H_2 or O_2 evolution from aqueous solutions on layered oxide photocatalysts consisting of Bi^{3+} with $6s^2$ configuration and d^0 transition metal ions. Chem Lett. 1999; 28: 1103-1104.

22. Xu L, Wan Y, Xie H, Huang Y, Qiao X, Qin L, Seo HL. On structure, optical properties and photodegradated ability of Aurivillius‐type Bi_3TiNbO_9 nanoparticles. J Am Ceram Soc. 2016; 99: 3964-3972.

23. Senthil V, Badapanda T, Chithambararaj A, Bose AC, Panigrahi S. Impedance spectroscopy and photocatalysis water splitting for hydrogen production with cerium modified $SrBi_2Ta_2O_9$ ferroelectrics. Int J Hydrogen Energy. 2016; 41: 22856-22865.

24. Yao WF, Xu XH, Wang H, Zhou JT, Yang XN, Zhang Y, Shang SX, Huang BB. Photocatalytic property of perovskite bismuth titanate. Appl Catal B-Environ. 2004; 52: 109-116.

25. Naresh G, Mandal TK. Excellent Sun-Light-Driven Photocatalytic Activity by Aurivillius Layered Perovskites, $Bi_{5-x}La_xTi_3FeO_{15}$ (x= 1, 2). ACS Appl Mater Inter. 2014; 6: 21000-21010.

26. Miranda C, Costa M, Avdeev M, Kholkin A, Baptista J. Relaxor properties of Ba-based layered perovskites. J Eur Ceram Soc. 2001; 21: 1303-1306.

27. Zhang H, Yan H, Reece MJ. High temperature lead-free relaxor ferroelectric: Intergrowth Aurivillius phase $BaBi_2Nb_2O_9$–$Bi_4Ti_3O_{12}$ ceramics. J Appl Phys. 2010; 107: 104111.

28. Kennedy B. Effect of temperature on cation disorder in $ABi_2Nb_2O_9$ (A= Sr, Ba). J Mater Chem. 1999; 9: 541-544.

29. Blake SM, Falconer MJ, McCreedy M, Lightfoot P. Cation disorder in ferroelectric Aurivillius phases of the type $Bi_2ANb_2O_9$ (A= Ba, Sr, Ca). J Mater Chem. 1997; 7: 1609-1613.

30. Kholkin A, Avdeev M, Costa M, Baptista J, Dorogovtsev S. Dielectric relaxation in Ba-based layered perovskites. Appl Phys Lett. 2001; 79: 662-664.

31. Taing J, Cheng MH, Hemminger JC. Photodeposition of Ag or Pt onto TiO_2 nanoparticles decorated on step edges of HOPG. ACS nano. 2011; 5: 6325-6333.

32. Patri SK, Deepti PL, Choudhary RNP, Behera B. Dielectric, impedance and modulus

spectroscopy of $BaBi_2Nb_2O_9$. J Electroceram. 2018; 40: 338-346.

33. Samara GA. The relaxational properties of compositionally disordered ABO_3 perovskites. J Phys: Condens Matter. 2003; 15: R367.
34. Cao J, Koval V, Zhang H, Lin Y, Wu J, Meng N, Li Y, Li Z, Zhang H, Yan H. Crystal structure and electrical properties of textured $Ba_2Bi_4Ti_5O_{18}$ ceramics. J Eur Ceram Soc. 2019; 39: 1042-1049.
35. Viola G, McKinnon R, Koval V, Adomkevicius A, Dunn S, Yan H. Lithium-induced phase transitions in lead-free $Bi_{0.5}Na_{0.5}TiO_3$ based ceramics. J Phys Chem C. 2014; 118: 8564-8570.
36. Wu J, Mahajan A, Riekehr L, Zhang H, Yang B, Meng N, Zhang Z, Yan H. Perovskite $Sr_x(Bi_{1-x}Na_{0.97-x}Li_{0.03})_{0.5}TiO_3$ ceramics with polar nano regions for high power energy storage. Nano Energy. 2018; 50: 723-732.
37. Kumar A, Kim SH, Peddigari M, Dong-Hyuk Jeong, Hwang GT, Ryu J. High energy storage properties and electrical field stability of energy efficiency of $(Pb_{0.89}La_{0.11})(Zr_{0.70}Ti_{0.30})_{0.9725}O_3$ relaxor ferroelectric ceramics. Electron Mater Lett. 2019; 15: 323-330.
38. Viola G, Tan Y, McKinnon RA, Wei X, Yan H, Reece MJ. Short range polar state transitions and deviation from Rayleigh-type behaviour in $Bi_{0.5}Na_{0.5}TiO_3$-based perovskites. Appl Phys Lett. 2014; 105: 102906.
39. Tauc J, Grigorovici R, Vancu A. Optical properties and electronic structure of amorphous germanium. Phys. Status Solidi B. 1966; 15: 627-637.
40. Silva CG, Juárez R, Marino T, Molinari R, García H. Influence of Excitation Wavelength (UV or Visible Light) on the Photocatalytic Activity of Titania Containing Gold Nanoparticles for the Generation of Hydrogen or Oxygen from Water. J Am Chem Soc. 2011; 133: 595-602.

Figure captions

Fig. 1 XRD pattern of the as-milled BBNO powders

Fig. 2 Particle size distribution of the as-milled BBNO powders. Inset: a typical SEM micrograph of the as-milled BBNO powders.

Fig. 3 *P*-*E* and *I*-*E* loops for BBNO ceramics measured at 10 Hz at different temperatures: (a) 200 °C; and (b) 25 °C. The *I*-*E* loops in both the first and second quadrants in Fig. (b) are replotted and shown in (c). The current peak positions shifted with increasing E_{max} along the two dotted green arrows.

Fig. 4 (a) UV-Vis absorption spectrum of BBNO and BBNO-Ag powders, where the dashed line represents the division between the UV and visible light regions; (b) the derived Tauc plot for BBNO, where the dashed line traces the linear part; (c) Degradation profiles for RhB with BBNO and BBNO-Ag under full light (100 mW/cm^2), visible-light blocking and UV light blocking.

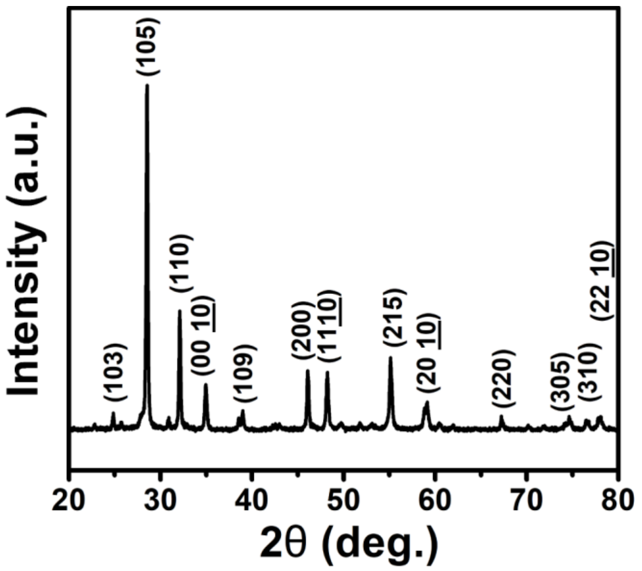
Intensity (a.u.)
(103)
(105)
(110)
(00 10)
(109)
(200)
(11 10)
(215)
(20 10)
(220)
(305)
(310)
(22 10)
20
30
40
50
60
70
80
2θ (deg.)

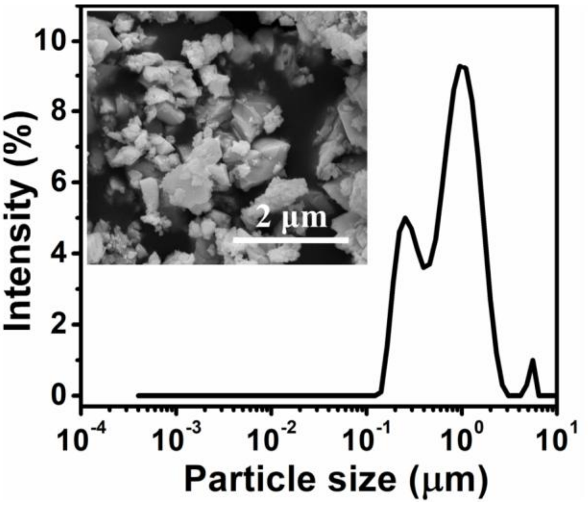
2 μm
Intensity (%)
0
2
4
6
8
10
Particle size (μm)
10^{-4}
10^{-3}
10^{-2}
10^{-1}
10^{0}
10^{1}

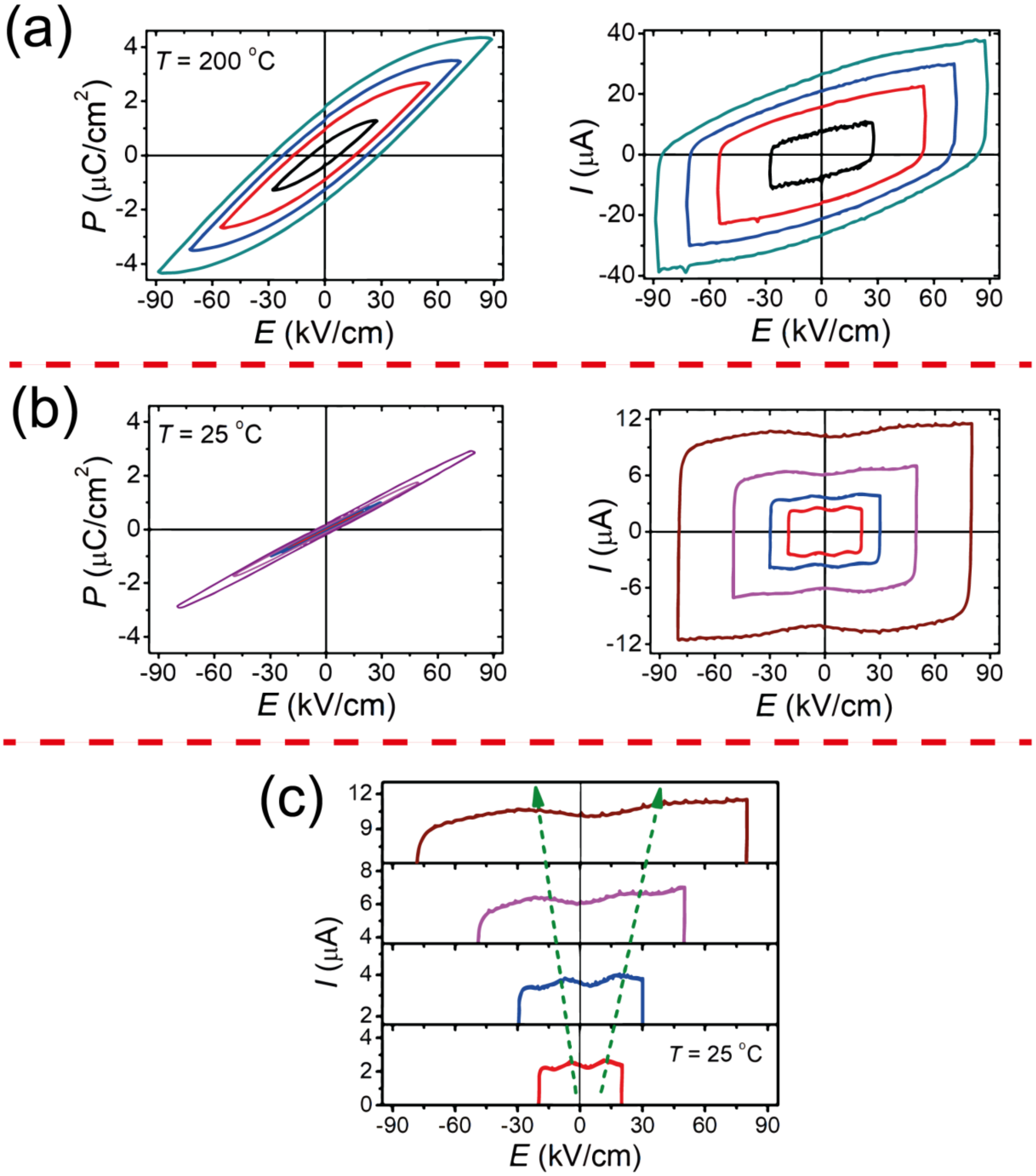
(a)
T = 200 °C
P (μC/cm²)
4
2
0
-2
-4
-90 -60 -30 0 30 60 90
E (kV/cm)
I (μA)
40
20
0
-20
-40
-90 -60 -30 0 30 60 90
E (kV/cm)
(b)
T = 25 °C
P (μC/cm²)
4
2
0
-2
-4
-90 -60 -30 0 30 60 90
E (kV/cm)
I (μA)
12
6
0
-6
-12
-90 -60 -30 0 30 60 90
E (kV/cm)
(c)
I (μA)
12
9
8
6
4
4
2
4
2
0
T = 25 °C
-90 -60 -30 0 30 60 90
E (kV/cm)

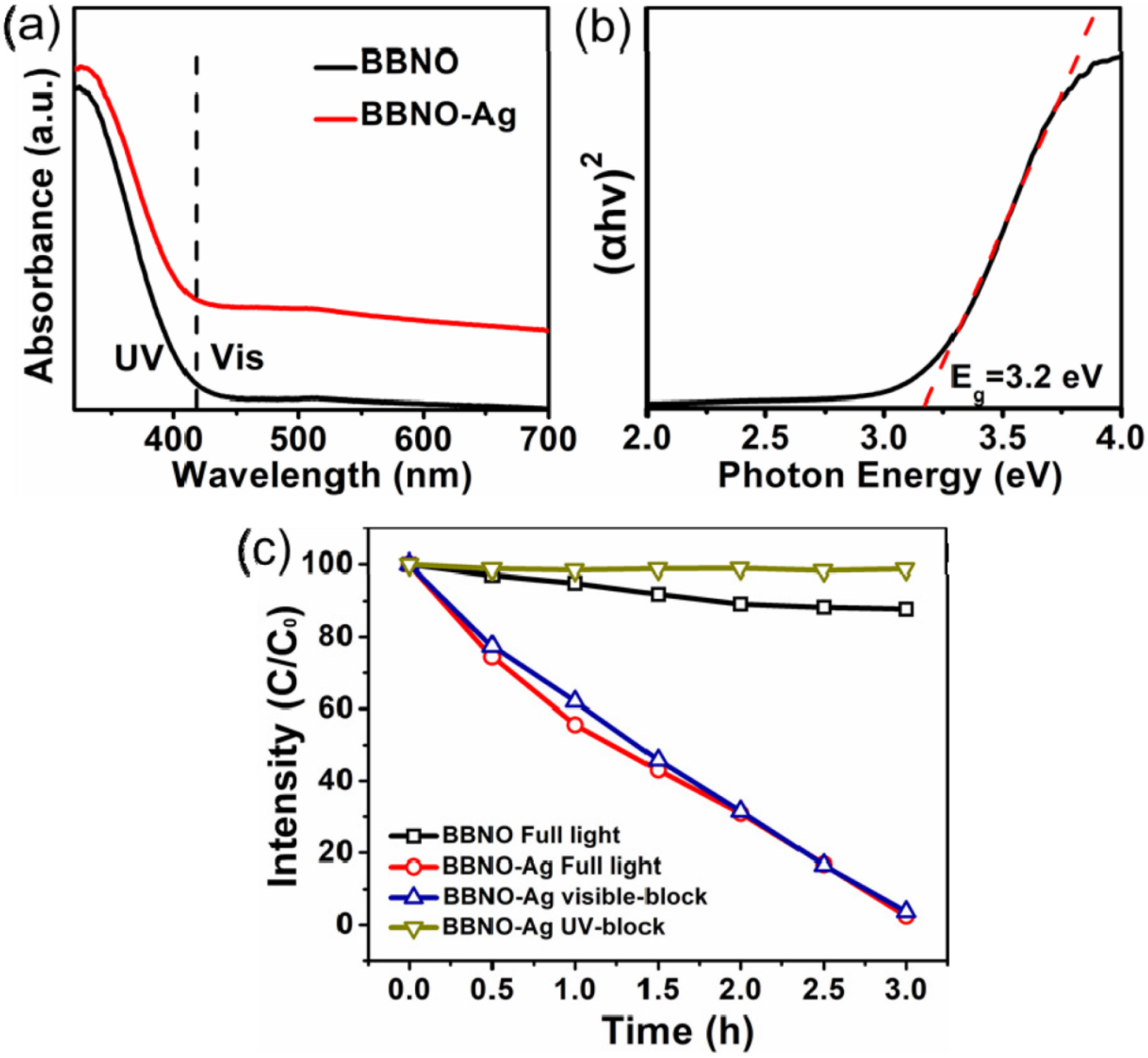
(a)
BBNO
BBNO-Ag
Absorbance (a.u.)
UV
Vis
400
500
600
700
Wavelength (nm)
(b)
$(\alpha h\nu)^2$
E_g=3.2 eV
2.0
2.5
3.0
3.5
4.0
Photon Energy (eV)
(c)
Intensity (C/C_0)
100
80
60
40
20
0
BBNO Full light
BBNO-Ag Full light
BBNO-Ag visible-block
BBNO-Ag UV-block
0.0
0.5
1.0
1.5
2.0
2.5
3.0
Time (h)